JOURNAL OF GEOPHYSICAL RESEARCH, VOL. 102, NO. D5, PAGES 5979–5991, MARCH 20, 1997

Results from the Intergovernmental Panel on Climatic Change Photochemical Model Intercomparison (PhotoComp)

Jennifer Olson,[1] Michael Prather,[2] Terje Berntsen,[3] Gregory Carmichael,[4] Robert Chatfield,[5] Peter Connell,[6] Richard Derwent,[7] Larry Horowitz,[8] Shengxin Jin,[9,10] Maria Kanakidou,[11] Prasad Kasibhatla,[12,13] Rao Kotamarthi,[14] Michael Kuhn,[15,16] Kathy Law,[17] Joyce Penner,[6,18] Lori Perliski,[19] Sanford Sillman,[20] Frode Stordal,[21] Anne Thompson,[22] and Oliver Wild[17]

Abstract. Results from the Intergovernmental Panel on Climatic Change (IPCC) tropospheric photochemical model intercomparison (PhotoComp) are presented with a brief discussion of the factors that may contribute to differences in the modeled behaviors of HO_x cycling and the accompanying O_3 tendencies. PhotoComp was a tightly controlled model experiment in which the IPCC 1994 assessment sought to determine the consistency among models that are used to predict changes in tropospheric ozone, an important greenhouse gas. Calculated tropospheric photodissociation rates displayed significant differences, with a root-mean-square (rms) error of the reported model results ranging from about ±6–9% of the mean (for O_3 and NO_2) to up to ±15% (H_2O_2 and CH_2O). Models using multistream methods in radiative transfer calculations showed distinctly higher rates for photodissociation of NO_2 and CH_2O compared to models using two-stream methods, and this difference accounted for up to one third of the rms error for these two rates. In general, some small but systematic differences between models were noted for the predicted chemical tendencies in cases that did not include reactions of nonmethane hydrocarbons (NMHC). These differences in modeled O_3 tendencies in some cases could be identified, for example, as being due to differences in photodissociation rates, but in others they could not and must be ascribed to unidentified errors. O_3 tendencies showed rms errors of about ±10% in the moist, surface level cases with NO_x concentrations equal to a few tens of parts per trillion by volume. Most of these model to model differences can be traced to differences in the destruction of O_3 due to reaction with HO_2. Differences in HO_2, in turn, are likely due to (1) inconsistent reaction rates used by the models for the conversion of HO_2 to H_2O_2 and (2) differences in the model-calculated photolysis of H_2O_2 and CH_2O. In the middle tropospheric "polluted" scenario with NO_x concentrations larger than a few parts per billion by volume, O_3 tendencies showed rms errors of ±10–30%. These model to model differences most likely stem from differences in the calculated rates of O_3 photolysis to $O(^1D)$, which provides about 80% of the HO_x source under these conditions. The introduction of hydrocarbons dramatically increased both the rate of NO_x loss and its model to model differences, which, in turn, are reflected in an increased spread of predicted O_3. Including NMHC in the simulation approximately doubled the rms error for O_3 concentration.

[1]NASA Langley Research Center, Hampton, Virginia.
[2]University of California, Irvine.
[3]University of Oslo, Oslo, Norway.
[4]University of Iowa, Iowa City.
[5]NASA Ames Research Center, Moffett Field, California.
[6]Lawrence Livermore National Laboratory, Livermore, California.
[7]Meteorological Office, Bracknell, Berkshire, England.
[8]Harvard University, Cambridge, Massachusetts.
[9]State University of New York at Albany.
[10]Now at New York State Department of Transportation, New York.
[11]Centre des Faibles Radioactivites, Gif-sur-Yvette, France.
[12]Georgia Institute of Technology, Atlanta.
[13]Now at MCNC/Environmental Programs, Research Triangle Park, North Carolina.
[14]AER, Inc., Cambridge, Massachusetts.
[15]Institute for Atmospheric Chemistry, Research Center Juelich, Juelich, Germany.
[16]Now at Fraunhofer Institut fuer Atmosphaerishche Umweltforschung, Garmisch-Partenkirchen, Germany.
[17]Cambridge University, Cambridge, England.
[18]Now at University of Michigan, Ann Arbor.
[19]Geophysical Fluid Dynamics Laboratory, Princeton, New Jersey.
[20]University of Michigan, Ann Arbor.
[21]Norwegian Institute for Air Research, Kjeller.
[22]NASA Goddard Space Flight Center, Greenbelt, Maryland.

Paper number 96JD03380.
0148-0227/97/96JD-03380$09.00

1. Introduction

Since preindustrial times there has been a steady increase in atmospheric concentrations of radiatively important greenhouse gases such as methane (CH_4) and carbon dioxide (CO_2) [*Keeling et al.*, 1982; *Kahlil and Rasmussen*, 1987]. These increases are expected to be paralleled by increased emissions of nitrogen oxides (NO_x= NO + NO_2) [*Dignon and Hameed*, 1989]. Photochemical reactions of these gases may generate tropospheric ozone (O_3) and, indeed, recent evidence suggests that concentrations of tropospheric O_3 have nearly doubled over the last century [*Volz and Kley*, 1988; *Harris et al.*, 1995]. Such O_3 increases will also tend to enhance the concentration of OH, which drives the removal of many major greenhouse gases. However, the concurrent growth of CH_4 has the opposite effect and will tend to suppress OH [*Thompson*, 1992]. The net effect on the chemical composition of the troposphere due to the increased emissions during the industrial era is a complex interaction between atmospheric constituents which is dependent on the physical state of the atmosphere (temperature and water vapor), transport and mixing, and chemical interactions.

In order to assess the ultimate chemical and radiative effects that such human-induced perturbations produce on a global scale, it is necessary to accurately model both the transport and the chemical responses of atmospheric gases to these perturbations. In 1994 the Intergovernmental Panel on Climate Change (IPCC) began intercomparisons of both tropospheric transport and photochemical models as a first step toward evaluating coupled global chemical transport models. We report here some of the results from the photochemical portion of that assessment (PhotoComp). For further information on the structure of the intercomparison the reader is referred to *Prather et al.* [1995] and *Stordal et al.* [1995].

PhotoComp was focused on elucidating the variability of results among published models, rather than being an attempt to intercompare, for instance, chemical mechanisms. Therefore, while the chemical mechanisms used in the various models were intentionally not standardized for this intercomparison, chemistry was limited to relatively simple, well-understood and agreed-upon gas-phase processes such as those described by *DeMore et al.* [1992]. Simulations including only CH_4 and carbon monoxide (CO) oxidation were examined separately from those also including nonmethane hydrocarbon (NHMC) oxidation to isolate differences that various NMHC chemistry parameterizations may introduce. There was no attempt to remove differences in model parameters such as kinetics data (rate constants), radiative transfer formulations, or chemical solvers. The goal of PhotoComp was to evaluate the consistency among models in the simulation of a simply characterized system in order to provide a necessary perspective in interpreting results from the more complicated IPCC model assessments. It should also be stressed that this intercomparison was structured to simulate only one process (i.e., gas-phase photochemistry) from the highly complex and interdependent system of processes present in the atmosphere. Dry deposition and in-cloud wet heterogeneous chemistry, for example, were neglected. In addition to the above stated goals we anticipate that the results presented in this paper should prove useful for modelers who wish to benchmark and evaluate the performance of their photochemical model in comparison with results from the several models presented here.

Input atmospheric and radiative parameters and initial conditions were strictly defined. Radiative calculations were specified as for clear-sky conditions with a solar zenith angle of 23° (July 1, 45°N latitude), a surface albedo of 10%, and an O_3 column equal to that given by the U.S. Standard Atmosphere profile. Six test cases were chosen to represent a range of atmospheric chemical regimes, and specifications for these are listed in Table 1. Conditions for the various cases were based loosely in part on measurements from missions that characterized the "remote" troposphere [e.g., *Ridley and Robinson*, 1992] and from those that sampled middle tropospheric pollution plumes such as those from biomass burning [e.g., *Harriss et al.*, 1988; *Fishman et al.*, 1996].

Twenty-one participants representing five countries responded with results for the cases with no NMHC chemistry (Marine, Land, Free, and Plume-X), and 16 of these groups

Table 1. PhotoComp Specifications and Initial Values

	Marine	Land Land-Bio	Free	Plume-X Plume-HC
Altitude, km	0	0	8	4
T, K	288.15	288.15	236.21	262.17
P, mbar	1,013.25	1,013.25	356.5	616.6
M molecules cm^{-3}	2.55×10^{19}	2.55×10^{19}	1.09×10^{19}	1.7×10^{19}
H_2O, % v/v	1.0	1.0	0.05	0.25
H_2, ppmv	0.5	0.5	0.5	0.5
H_2O_2, ppbv	2	2	2	2
O_3, ppbv	30	30	100	50
NO_x, pptv[a]	10	200	100	10,000
HNO_3, pptv	100	100	100	100
CO, ppbv	100	100	100	600
CH_4, ppbv	1,700	1,700	1,700	1,700
NMHC	none	land, 0 bio, 1 ppbv isoprene	none	X, 0 HC, 115 ppbv[b]

Integrations were performed for 5 days starting July 1, with solar zenith angle 23°.

[a]NO_x initially equally divided between NO and NO_2.

[b]Initial values of NMHC for PLUME-HC (in pbbv): C_2H_6, 25; C_2H_4, 40; C_2H_2, 15; C_3H_8, 15; C_3H_6, 12.5; C_4H_{10}s, 5; toluene, 2; and isoprene, 0.5.

additionally submitted results for the two cases that include NMHC chemistry (Land-Bio and Plume-HC). Table 2 lists these participating groups and contact information. The participants were given initial conditions at noon and were asked to simulate a 5-day period for an isolated chemical system with a diurnal solar cycle. Submitted diagnostics were the predicted noontime values of constituent concentrations, the diurnally averaged values of some radical species (e.g., HO_2 and NO_3), and photolysis rates. We present here a review of the results from the PhotoComp exercise and discuss the likely sources of variation between the model results. In particular, our analysis emphasizes the cases without NMHC and focuses on the relation between O_3 and HO_x.

2. Brief Review of HO_x/O_3 Interactions

The odd-hydrogen radicals (HO_x = OH + HO_2) are central to tropospheric chemistry: the major sink for many atmospheric greenhouse gases is reaction with OH, and HO_2 is the essential HO_x catalyst in the production and loss of tropospheric O_3. It is thus necessary to understand the chemical cycling of HO_x and HO_x reservoirs such as H_2O_2 in the troposphere. Concentrations of OH and HO_2 may vary by orders of magnitude over the course of a day, because they respond rapidly to changes in incoming solar radiation. HO_x concentrations are also dependent on abundances of trace gases such as water vapor, O_3, CO, CH_4, NO_x, and NMHC. Aqueous-phase chemistry within clouds is likely to have an additional significant global impact on HO_2 concentrations (this process is neglected in PhotoComp) [e.g., *Lelieveld and Crutzen*, 1990; *Möller and Mauersberger*, 1992]. Although intensive measurement campaigns [e.g., *Perner et al.*, 1987; *Salawitch et al.*, 1994] can test OH and HO_2 calculations under specific circumstances, we are unable to measure the global distribution of OH except as an indirect, integrated quantity [e.g., *Prinn et al.*, 1995]. Therefore we will continue to rely on models to predict global HO_x concentrations and the oxidizing capacity of the troposphere.

The primary source of HO_x in the natural troposphere is from the reaction of metastable atomic oxygen $O(^1D)$ with water vapor to form the hydroxyl radical (OH) (R3). There are also secondary HO_x sources from the photolysis of aldehydes ((R4), for example) and hydrogen peroxide (H_2O_2) (R5), although note that these sources originate from HO_x.

$$O_3 + h\nu \rightarrow O(^1D) \quad \text{(R1)}$$

$$O(^1D) + M + O_2 \rightarrow O_3 \quad \text{(R2)}$$

$$O(^1D) + H_2O \rightarrow 2OH \quad \text{(R3)}$$

$$CH_2O + h\nu + \text{fast steps} \rightarrow 2HO_2 + CO \quad \text{(R4)}$$

$$H_2O_2 + h\nu \rightarrow 2OH \quad \text{(R5)}$$

The abundance of HO_x further depends on NO_x concentrations. For NO_x larger than several parts per billion by volume (ppbv), NO_x acts primarily as a reducing compound such that the major HO_x sink is reaction of OH with NO_2 to form the reservoir HNO_3. For lower NO_x concentrations the major HO_x sink is the self-reaction of HO_2 to form the reservoir H_2O_2 [*Liu et al.*, 1987; *Lin et al.*, 1988; *Sillman et al.*, 1990; *Kleinman*, 1991]. For the remainder of this paper we loosely define the former as a "high- NO_x regime" (with respect to the HO_x cycle) and the latter as a "low- NO_x regime." The isolated chemical system defined by PhotoComp includes no transport or irreversible losses of H_2O_2 or HNO_3 (e.g., washout), so that photolysis of the reservoir species may eventually (but not necessarily in 5 days) return the HO_x and NO_x back to the system.

The important reactions responsible for O_3 destruction in the natural troposphere are directly related to HO_x chemistry,

Table 2. PhotoComp Participants

Affiliation	Contact
AER, Inc. (box model code)	Rao Kotamarthi: rao@aer.com
AER, Inc. (2-D code)	Rao Kotamarthi: rao@aer.com
Cambridge University (box model code)	Oliver Wild: oliver@atm.ch.cam.ac.uk
Cambridge University (UGAMP code)	Kathy Law: kathy@atm.ch.cam.ac.uk
Centre des Faibles Radioactivites	Maria Kanakidou: mariak@obelix.saclay.cea.fr
Georgia Institute of Technology	Prasad Kasibhatla: psk@hpcc.epa.gov
GFDL	Lori Perliski: lmp@gfdl.gov
Harvard University	Larry Horowitz: lwh@europa.harvard.edu
Forschungszentrum Juelich	Michael Kuhn: kuhn@ifu.fhg.de
LLNL (2-D code)	Peter Connell: connell2@llnl.gov
LLNL(3-D code)	Joyce Penner: joyce_penner@umich.edu
NASA Ames	Robert Chatfield: chatfield@clio.arc.nasa.gov
NASA Goddard	Anne Thompson: thompson@gator1.gsfc.nasa.gov
NASA Langley	Jennifer Olson: j.r.olson@larc.nasa.gov
Norwegian Institute for Air Research	Frode Stordal: frode@zardoz.nilu.no
NYU-Albany	Shengxin Jin: sjin@gw.dot.state.ny.us
U.C. - Irvine	Michael Prather: prather@halo.ps.uci.edu
University of Iowa	Gregory Carmichael: gcarmich@icaen.uiowa.edu
U.K. Met. Office	Richard Derwent: rgderwent@email.meto.govt.uk
University of Michigan	Sanford Sillman: sillman@kudzu.sprl.umich.edu
University of Oslo	Terje Berntsen: terje.berntsen@geofysikk.uio.no

AER, Atmospheric and Environmental Research; UGAMP, Universities Global Atmospheric Modelling Programme; GFDL, Geophysical Fluid Dynamics Laboratory; LLNL, Lawrence Livermore National Laboratory; NASA, National Aeronautics and Space Administration; NYU, New York University; U.C. - Irvine, University of California - Irvine; U.K. Met. Office, United Kingdom Meteorological Office.

as is the photochemical smog reaction that produces O_3. Noted above, the photolysis of O_3 to $O(^1D)$ can lead to O_3 loss by the sequence (R1) + (R3), especially within the moist lower troposphere. The direct reactions of HO_x with O_3 also represent major loss,

$$HO_2 + O_3 \rightarrow OH + 2\,O_2 \quad \text{(R6)}$$

$$OH + O_3 \rightarrow HO_2 + O_2 \quad \text{(R7)}$$

while those with NO_x can catalytically produce O_3.

$$HO_2 + NO \rightarrow OH + N\,O2 \quad \text{(R8)}$$

$$NO_2 + h\nu + O_2 \rightarrow NO + O3 \quad \text{(R9)}$$

Here we examine HO_x cycling in the PhotoComp simulations without NMHC to determine whether the model to model differences in O_3 tendencies can be traced to (1) photolysis rates, (2) related HO_x chemical mechanisms, or (3) other hidden differences in formulation or numerical solution.

3. Summary of Results

3.1. Photolysis Rates

The mean values and 1 rms error for the four selected photolytic reactions are listed in Table 3 for four altitudes.

Note that

$$\text{rms error} = \sqrt{\sum (C_i - C_{mean})^2 / N}$$

where C_i is the individual model results, C_{mean} is the mean of model results, and N is the number of models. These values were calculated from 20 of the models, discarding one obvious outlier. The rms errors (as a percentage of the mean) are largest for CH_2O and H_2O_2 photolysis, with values of the order of 10–15%. Errors for these two rates systematically increase with altitude. Root-mean-square errors for NO_2 and O_3 photolysis are generally less than 9%. The errors (as a percentage of the mean) tend to be slightly larger for the diurnally averaged rates, reflecting the magnification of technique-dependent errors with higher zenith angle and longer optical path lengths.

The majority of the models used quantum yields and cross-section data from the Jet Propulsion Laboratory recommendations of *DeMore et al.* [1992]. Five models used data recommended by various earlier references, but any dependence of the differences in photodissociation rates between the models on the choice of photokinetics data used was apparently masked by other larger dependencies.

The effect of multiple scattering on photodissociation rates is expected to be significant for molecules whose absorption cross sections are large above about 300 nm [e.g., *Meier et al.*, 1982]. Below this wavelength, absorption accounts for most of the radiative transfer process. For the molecules considered in PhotoComp, multiple scattering is most likely to enhance the photodissociation rates of NO_2 and CH_2O, which are driven by wavelengths longer than 320 nm, while it should have a lesser effect on those of O_3 (to $O(^1D)$) and H_2O_2, which emphasize the shorter wavelengths near 310 nm.

The models participating in PhotoComp may be broadly separated into two groups: those using multistream methods of radiative transfer to account for scattering and those using some form of a two-stream method. Specific types of two-stream methods represented by one or more models in PhotoComp include collimated [e.g., *Isaksen et al.*, 1977], isotropic [e.g., *Luther*, 1980], and delta or delta-Eddington [e.g., *Madronich*, 1987]. Of the 20 models represented in Table 3, 16 employed one of the two-stream approximations, and four used multistream approximations.

Table 3. Photolysis Rates From PhotoComp Models

	$O_3 + h\nu \rightarrow O(^1D) + O_2$	$NO_2 + h\nu \rightarrow NO + O$	$H_2O_2 + h\nu \rightarrow OH + OH$	$CH_2O + h\nu \rightarrow H + CHO$
		Noon		
Surface	$2.70\ (\pm.18) \times 10^{-5}$ (±6.7%)	$0.91\ (\pm.06) \times 10^{-2}$ (±6.1%)	$7.38\ (\pm.55) \times 10^{-6}$ (±7.4%)	$3.00\ (\pm.29) \times 10^{-5}$ (±9.7%)
4 km	$3.47\ (\pm.22) \times 10^{-5}$ (±6.4%)	$1.08\ (\pm.08) \times 10^{-2}$ (±7.2%)	$9.47\ (\pm.93) \times 10^{-6}$ (±9.8%)	$4.11\ (\pm.52) \times 10^{-5}$ (± 2.6%)
8 km	$3.38\ (\pm.23) \times 10^{-5}$ (±6.8%)	$1.16\ (\pm.08) \times 10^{-2}$ (±7.0%)	$10.20\ (\pm 1.23) \times 10^{-6}$ (±12.1%)	$4.64\ (\pm.61) \times 10^{-5}$ (±13.2%)
12 km	$3.08\ (\pm.19) \times 10^{-5}$ (±6.3%)	$1.18\ (\pm.08) \times 10^{-2}$ (±6.6%)	$10.38\ (\pm 1.42) \times 10^{-6}$ (±13.7%)	$4.81\ (\pm.61) \times 10^{-5}$ (±12.6%)
		Diurnal Average		
Surface	$0.71\ (\pm.05) \times 10^{5}$ (±7.2%)	$0.39\ (\pm.03) \times 10^{2}$ (±7.1%)	$2.67\ (\pm.22) \times 10^{6}$ (±8.3%)	$1.04\ (\pm.11) \times 10^{5}$ (±10.8%)
4 km	$0.94\ (\pm.08) \times 10^{5}$ (±8.0%)	$0.50\ (\pm.02) \times 10^{2}$ (±7.8%)	$3.65\ (\pm.39) \times 10^{6}$ (±10.6%)	$1.52\ (\pm.21) \times 10^{5}$ (±14.0%)
8 km	$0.94\ (\pm.08) \times 10^{5}$ (±8.6%)	$0.57\ (\pm.02) \times 10^{2}$ (±7.2%)	$4.18\ (\pm.50) \times 10^{6}$ (±12.0%)	$1.83\ (\pm.26) \times 10^{5}$ (±14.0%)
12 km	$0.86\ (\pm.07) \times 10^{5}$ (±8.0%)	$0.61\ (\pm.01) \times 10^{2}$ (±7.4%)	$4.49\ (\pm.58) \times 10^{6}$ (±13.0%)	$2.00\ (\pm.27) \times 10^{5}$ (±13.5%)

Values are mean (per second) ±1 rms error (and rms error as percentage of mean).

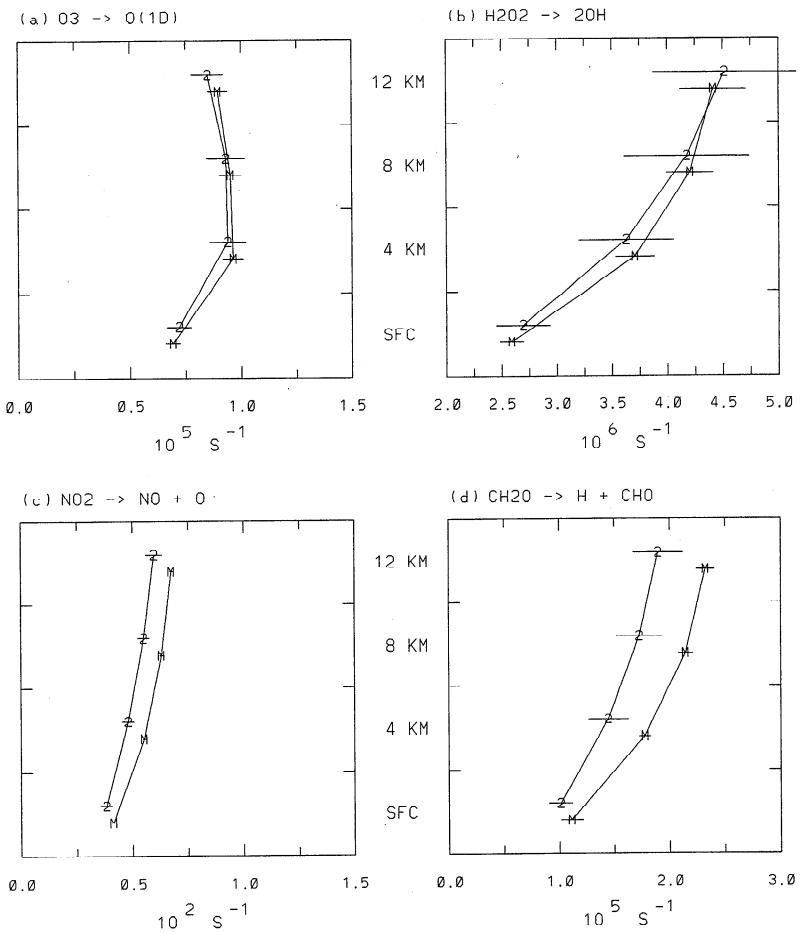

Figure 1. Photodissociation rates calculated by multistream and two-stream radiative transfer models. The mean photodissociation rate (inverse seconds) and ±1 rms error (horizontal lines) are calculated for four altitudes (ordinate axis) and are shown for those models using two-stream methods of radiative transfer (indicated by the 2) and those using multistream methods (indicated by the M). Results are shown for (a) O_3 photolysis to $O(^1D)$, (b) H_2O_2 photolysis, (c) NO_2 photolysis, and (d) CH_20 photolysis. Note that the scales vary for each figure.

Figure 1 shows a comparison of diurnally averaged photodissociation means and rms errors for the two-stream and multistream classifications. While there are essentially no differences in the mean rates for O_3 and H_2O_2 (Figures 1a and 1b), the models using multistream code calculate distinctly larger rates for NO_2 and CH_2O (Figures 1c and 1d). When we remove this bias from the statistics calculations, the rms errors for the diurnally averaged rates are reduced by about one third to between 10% and 11% at all altitudes for CH_2O and to between 4% and 5% for NO_2 photolysis. There are no corresponding significant changes in the errors for O_3 or H_2O_2.

3.2. Species Concentration

The 5-day sequence of computed mixing ratios for noontime O_3 and NO_x are in Figures 2–5 for the six PhotoComp cases. The figures show a basic dependence of the net O_3 tendency on NO_x concentration. Although the cases span a variety of atmospheric altitudes and conditions, in general, the tendency is negative when NO_x is less than a few tens of parts per trillion volume (pptv) and positive for higher concentrations. Conservation of the sum $NO_x + HNO_4 + HNO_3$ was checked for the surface simulations, and all but two of the models conserved this quantity to better than 99%. The remaining two conserved to better than 95%.

Figures 2–5 show the mean of the 21 individual model results for each day and a ±1 rms error envelope (dashed lines). The median model value for each day is also shown by an asterisk. Mean and median values were similar in all of the cases without NMHC chemistry (differences of less than 5%; Figures 2 and 3). The two cases with hydrocarbons (Land-Bio and Plume-HC) gave more widely divergent results, in part because of the lack of an agreed-upon standard mechanism and rates, as have been developed for stratospheric chemistry [e.g., *DeMore et al.*, 1992]. For example, the O_3 and NO_x means and medians diverge by as much as 25% (Figures 4 and 5). Note that results from two of the models participating in the hydrocarbon cases were discarded for this analysis because their reported values of NO_x were as much as 500 times larger than those from the remaining models.

In the upper troposphere Free case (Figure 3), with moderate-to-low NO_x values (primarily around 20 to 40 pptv after the first day), there is a slow net destruction of O_3 of only

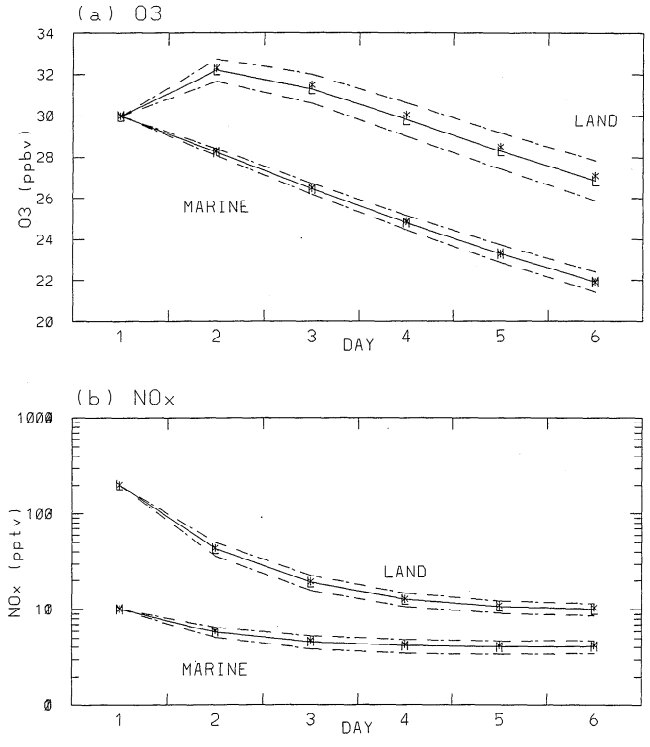

Figure 2. Mean and 1 rms error for O_3 and NO_x from the Marine and Land cases. The mean of the reported noontime values for (a) O_3 in ppbv and (b) NO_x in pptv is shown by the solid line. Results from the Marine case are indicated with the M, and results from the Land case are shown with the L. Note that the axis for NO_x mixing ratio is logarithmic. Day 1 (along the abscissa) shows the initial value for the start day, and results are shown for each day of the 5-day run (days 2–6). A ±1 rms envelope is shown with dashed lines. Median values for each day are shown with an asterisk.

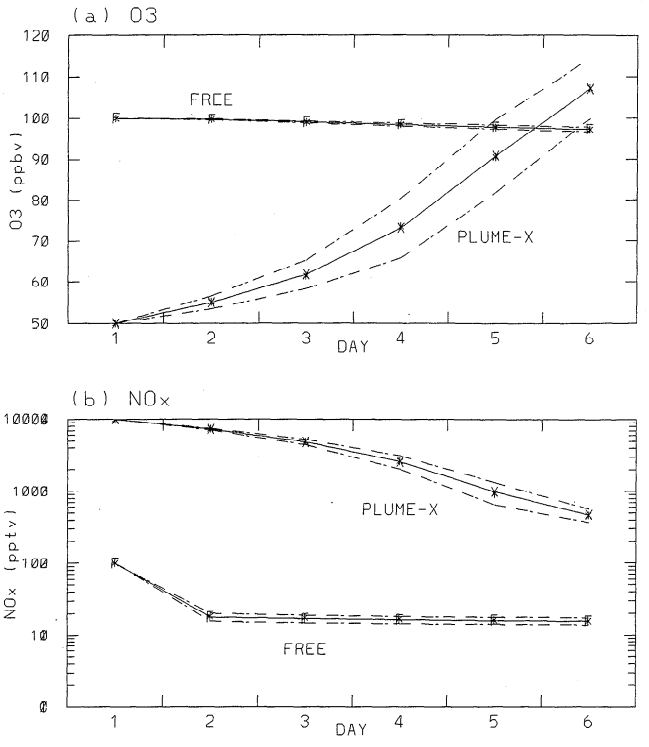

Figure 3. Same as figure 2 for the Free (F) and Plume-X cases (X).

slightly more than 0.5 ppbv d^{-1}. Because of this slower rate of chemistry the rms error around the mean concentrations is less for this particular simulation than for the other simulations with faster rates of oxidant formation: the rms error is less than 1% of the mean for O_3 and less than 15% for NO_x. The rms error for the O_3 tendency, however, is near 0.1 ppbv d^{-1}, which is of the order of 20% of the 0.5 ppbv d^{-1} decay rate.

The surface level, low-NO_x (<10 pptv) Marine results (Figure 2) show a consistent trend of O_3 decreasing by between 1.5 and 2 ppbv d^{-1}. In the similar Land case the higher initial concentrations of NO_x (200 pptv) produce an O_3 increase of about 2 ppbv during the first day. Once NO_x concentrations fall to less than 20 pptv during the latter several days of the Land case, the ozone decrease parallels that of the Marine case, but with an offset of +5 ppbv. These two cases are identical except for the initial NO_x and serve as a sensitivity test: the additional 190 pptv of NO_x produces a net 5 ppbv of O_3, or a yield of about 26 molecules of O_3 per molecule of NO_x.

The largest model to model differences in the predicted O_3 concentrations are those for the Plume-X and Plume-HC cases (Figures 3 and 5), with an rms error typically 10–15% of the mean. This is accompanied by a significant scatter in predicted NO_x, which is of the order of ±100 pptv for the Plume-X case. The results from the Plume-X case show higher NO_x concentrations (>500 pptv) throughout the 5-day period and show O_3 increasing significantly from an early rate of 5 ppbv d^{-1} to more than 15 ppbv d^{-1} during the last few model days. The introduction of hydrocarbons (Plume-HC) has a significant impact on the NO_x lifetime and O_3 production. Because of the presence of hydrocarbon oxidation products the subsequent formation of nitrates such as peroxyacetyl nitrate (PAN) as an important reservoir of NO_x rapidly depletes ambient NO_x. While NO_x in the Plume-X case (Figure 3) remains above 1 ppbv for much of the period, it drops to about 50 pptv after only 1 day of integration when NMHC chemistry is considered (Figure 5). As a result the behavior of O_3 is dramatically altered in the Plume-HC case, with an initial increase of 100 ppbv followed by a steady decline in concentration when NO_x levels are typically 20 pptv. Extrapolating back to day 1, the net O_3 yield for this scenario is about 8 to 10 molecules per molecule of NO_x, much less than the amount for the unpolluted surface layer.

Although the model to model differences are not excessively large for the low-NO_x surface Marine and Land cases, it is important to understand why the models differ in these predicted O_3 destruction rates, since most global tropospheric O_3 photochemical destruction occurs in the moist lower troposphere. The mean net O_3 tendency simulated by the models through the last day of integration is about -1.5 ppbv d^{-1} for both Marine and Land cases. The model to model rms errors of these loss rates are about 10% of the means, a finding that implies that about one third of the models are predicting O_3 tendencies more than ±10% from the mean, even though they are all simulating identical conditions. Possible explanations for some of these differences are discussed in the next section.

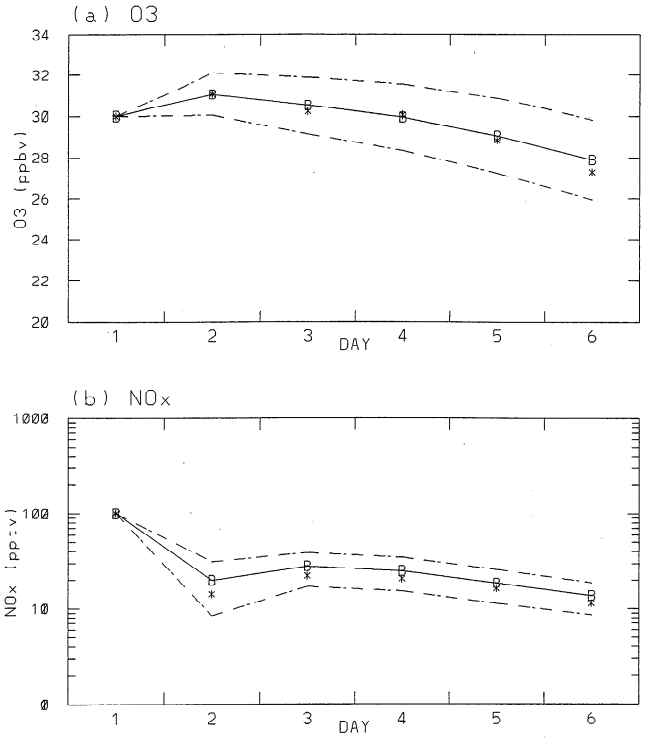

Figure 4. Same as figure 2 for the Land-bio case (B).

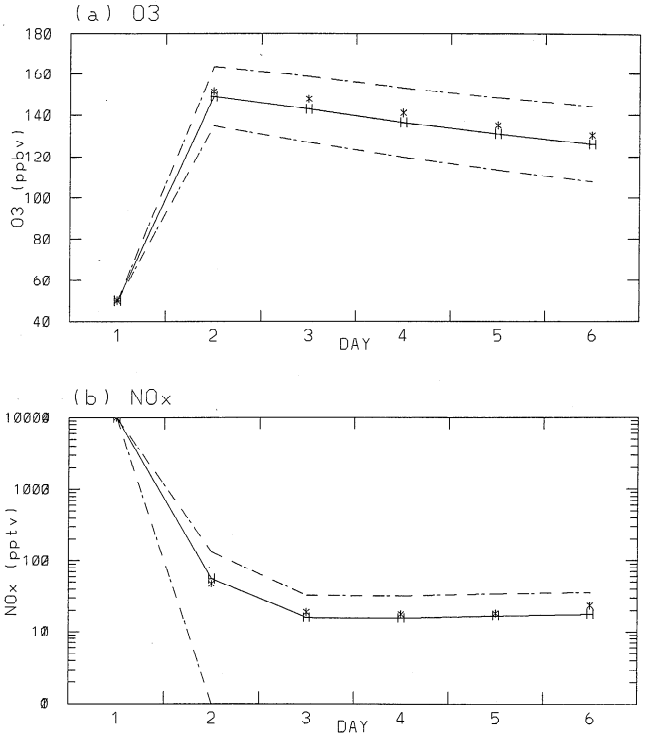

Figure 5. Same as figure 2 for the Plume-HC case (H).

4. Analysis of Model to Model Differences

4.1. Surface Cases

The 5-day sequence of individual model mixing ratios of noontime O_3 and H_2O_2, and diurnally averaged HO_2 and OH for the surface level Marine case, are shown in Figure 6. The general patterns of behavior presented here are also similar to the Land and (to some extent) the Land-Bio cases. For the purpose of this analysis, three subsets of consistent model behaviors were identified. In general, the subsets were defined as groups of models that displayed similar relative abundances of HO_x and O_3. Characteristics of the subsets are described in more detail below. The factors contributing to the different behaviors of these subsets explain much of the total model to model variance shown in Figures 2–5.

The individual model results in Figure 6 are identified by a subset group number. Note that four of the models do not display behavior consistent with any of these three subsets and are denoted with an asterisk. When the results are plotted in this fashion, an apparent relation between the O_3 tendencies and diurnally averaged HO_2 becomes evident (Figures 6a and 6c). That is, subsets with the highest HO_2 concentrations (subsets 1 and 3) show the fastest O_3 destruction rates. A correlation coefficient (r) equal to -0.53 (significant to >99%) was calculated between differences from the mean of the individual model O_3 loss rates during each day of the simulation and the accompanying differences in the HO_2 concentration. Alternately, model to model differences from the mean of the photolysis of O_3 (to $O(1D)$) were not found to have a significant correlation to the differences in the O_3 loss rate.

The loss frequency of O_3 due to direct reaction with HO_2, (R6), is calculated here from the product of the rate constant [*DeMore et al.*, 1992] and the reported diurnally averaged HO_2 from each model, giving a mean value of 3.1×10^{-7} s^{-1} (-0.8 ppbv d^{-1}). This corresponds to about one half the total net O_3 loss frequency. The model to model rms error of this single loss, 0.4×10^{-7} s^{-1}, constitutes about 80% of the rms error for the total net O_3 loss. We conclude that differences in the predicted loss rates for O_3 in the surface cases can be largely traced to the HO_2 concentrations.

Both subsets 2 and 3 indicate a positive relation between differences in HO_2 and H_2O_2 from their respective means, with subset 3 showing larger concentrations of both constituents. In contrast, subset 1 clearly shows the lowest concentrations of H_2O_2 (Figure 6b) along with the highest concentrations of HO_2. Evidently, for subset 1 the exchange between HO_x and H_2O_2 is shifted in favor of HO_x. There is no apparent consistency in the differences in the rate of H_2O_2 photolysis for the models in subset 1; these results span the entire range of reported rates (see Figure 7b). *Stockwell* [1995] stressed the importance of including the pressure and water vapor dependence of the $HO_2 + HO_2$ reaction to form H_2O_2 in atmospheric chemistry models, because omitting them can result in a relative error near the surface as high as 75% [*Kircher and Sander*, 1984]. The resulting effect is lower H_2O_2 production and a relatively increased HO_2 concentration. For the conditions in this PhotoComp case, omission of the water vapor dependence reduces the conversion of HO_2 to H_2O_2 by 35%. It was subsequently verified that the models in subset 1 do not include this H_2O dependence of the HO_2 self reaction.

Examination of subsets 2 and 3 reveals that differences in OH from the mean (Figure 6d) generally display a positive relation to differences from the mean for both H_2O_2 and HO_2. As was discussed earlier, the photolysis of O_3 is the primary source of HO_x, and photolysis of H_2O_2 and CH_2O is an important pathway in the regeneration of HO_x from HO_x

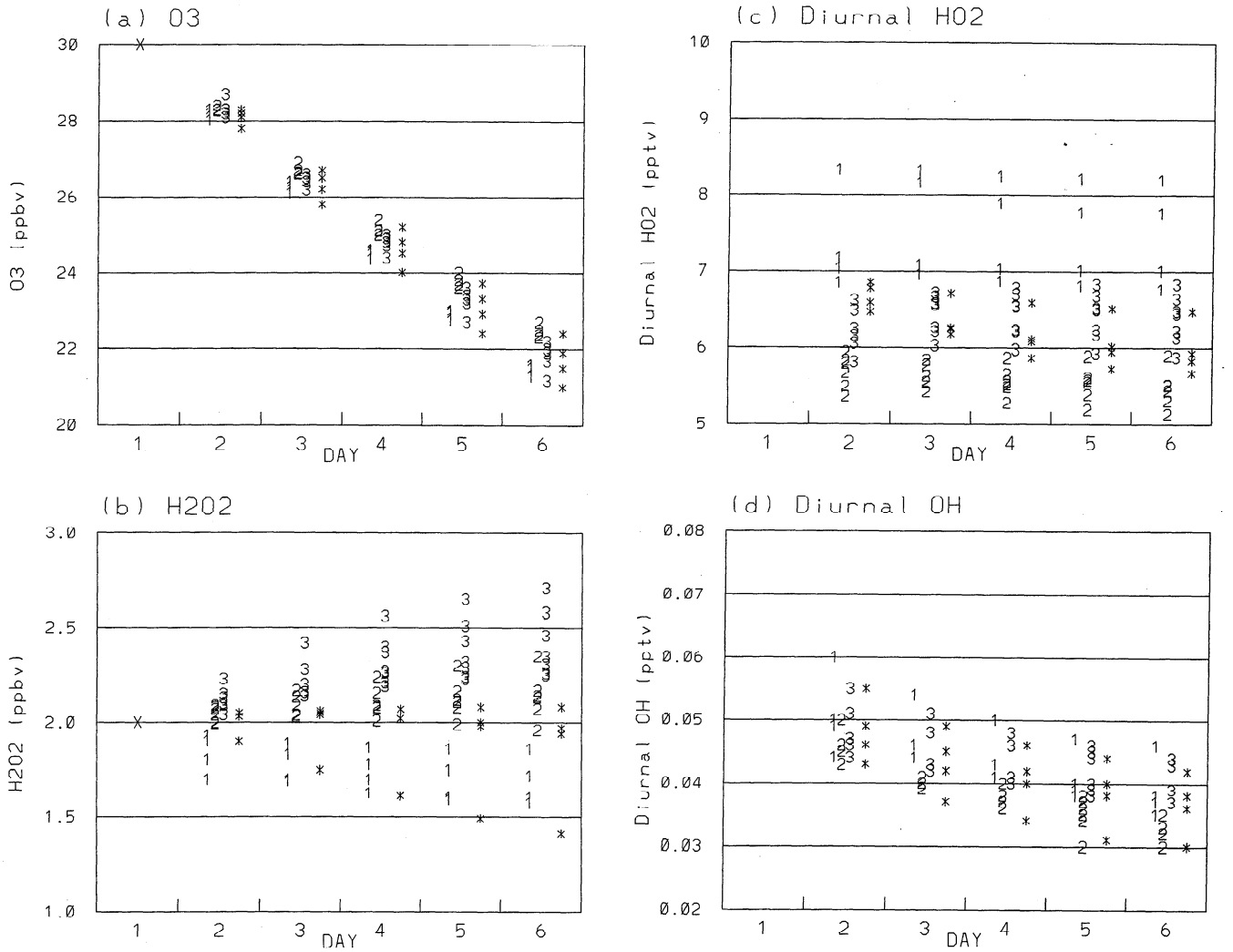

Figure 6. Individual model results for the Marine case. Each model is identified with a subset number 1, 2, or 3. Models that don't fit into any subset are shown with an asterisk. Noontime values for each day of the simulation (along the abscissa) are shown for (a) O_3 in ppbv and (b) H_2O_2 in ppbv. Diurnally averaged values for the previous 24 hours are shown for (c) HO_2 in pptv and (d) OH in pptv.

reservoir species. A cursory examination of diurnally averaged photolysis rates used by the models in subsets 2 and 3 (Figure 7) suggests that with one or two exceptions there is a tendency for subset 2 models to calculate slightly slower rates than subset 3 for the photodissociations of H_2O_2 and CH_2O in the boundary layer. The diurnally averaged production of HO_x from each of these pathways was estimated for the last day of model integration by using the appropriate model reported concentrations and diurnally averaged photolysis rates. These are shown in Table 4, along with calculated correlations between the photolysis rates that drive the production pathways and HO_2 concentrations. As expected, the dominant production of HO_x is the pathway initiated by the photolysis of O_3. However, the largest rms errors are calculated for the sources from H_2O_2 and CH_2O photolysis, and the model to model differences in HO_2 are most closely correlated with differences in the photolysis rate of these constituents.

The behaviors of these subsets imply that for the surface, low-NO_x PhotoComp regimes, differences between the models in HO_x are the dominant factors leading to the varying O_3 loss rates. Differences in HO_2 are likely due to (1) inconsistencies in the conversion rate of HO_2 to H_2O_2 and (2) variations in HO_x sources from reservoir species, such as differences in the H_2O_2 and CH_2O photolysis rates. Note that as discussed previously, H_2O_2 photolysis rates, while showing rms errors of the order of 8% of the mean near the surface, did not show a systematic dependence on the choice of multistream versus two-stream radiative code or on the choice of photokinetics data used by the models. However, the choice of multistream versus two-stream radiative code contributed about one third of the rms error associated with the rate for CH_2O photodissociation. Additional contributions to differences between the models could be due to a combination of factors such as choice of time steps, which range from 1 s to several hours for the models represented here, or numerical solvers used, although the recent work of *Stolarski et al.* [1995] suggests that this makes little difference.

4.2. Plume-X Case

Results from the Plume-X simulation (Figure 8) show clear changes in HO_x chemistry as NO_x concentrations decrease from an initial value of 10 ppbv to less than 1 ppbv after

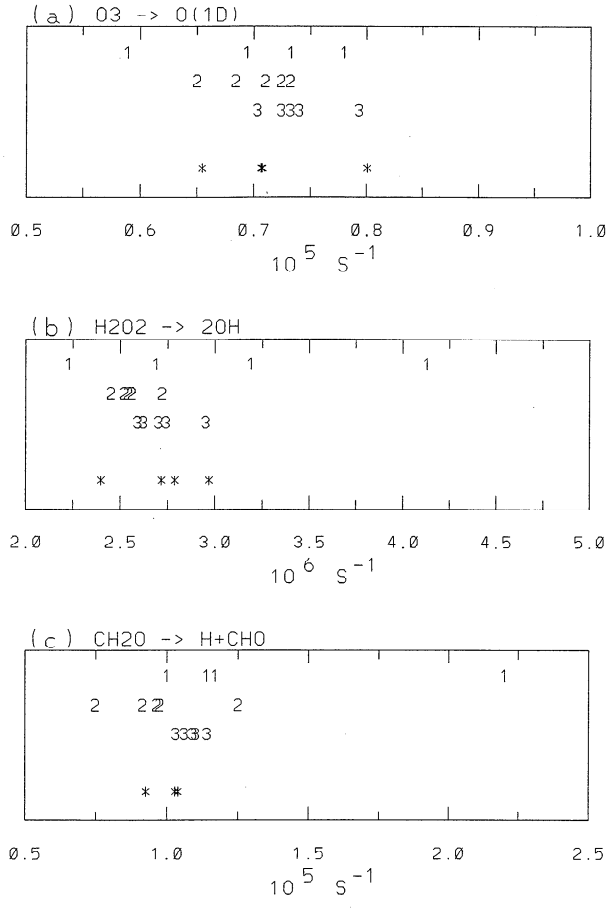

Figure 7. Diurnally averaged photolysis rates at the surface. Rates are shown in inverse seconds for the diurnally averaged surface level photolysis rate for (a) O_3 (to $O(^1D)$), (b) H_2O_2, and (c) CH_2O. Each model is identified with a subset number 1, 2, or 3 or with an asterisk, as in Figure 6.

5 days (Figure 8b). Concentrations of NO_x greater than 2 ppbv throughout the first part of the simulation suppress HO_x radicals (Figure 8c) due to rapid formation of nitric acid (HNO_3).

$$NO_2 + OH \rightarrow HNO_3 \qquad (R10)$$

The growth rate of HNO_3 (not shown) is initially 2.5 to 3 ppbv d^{-1} but slows to <1 ppbv d^{-1} toward the end of the simulation as NO_x concentrations decrease. The transition from a "high-NO_x" to a "low-NO_x" regime is also reflected in the behavior of H_2O_2 (not shown). The initial net tendency of H_2O_2 is to decrease while total HO_x is suppressed, but as NO_x concentrations fall and HO_x increases, H_2O_2 reverses trend and begins to increase as its production rate becomes larger than its photolytic destruction.

A secondary effect of the "high-NO_x" regime is an increased OH:HO_x ratio (Figure 8d), because the OH:HO_2 balance is strongly controlled by the conversion of HO_2 to OH by NO (R8). After NO_x concentrations fall below 2 ppbv at the end of the simulation, HO_x radicals increase dramatically, and the OH:HO_x ratio also begins to decrease.

O_3 concentrations increase consistently throughout the simulation (Figure 8a), but the increase is more rapid after the NO_x levels fall and HO_x recovers. There has been much discussion in the literature concerning O_3 production efficiency as a function of NO_x concentration [e.g., *Liu et al.*, 1987; *Lin et al.*, 1988; *Sillman et al.*, 1990; *Fehsenfeld and Liu*, 1993]. For these simple, no-NMHC conditions, this efficiency is directly related to the OH:HO_x ratio and the HO_x radical concentration. Under high-NO_x conditions, HO_x radicals are suppressed, and OH:HO_x ratios increase. This effect causes the rate of NO_x removal (via conversion to HNO_3, (R7)) to be large in relation to the initial step in the O_3 production process (conversion of NO to NO_2, (R8)). The result is a lower O_3 production efficiency, defined as the ratio of O_3 formation to NO_x removal.

The model to model rms error in O_3 production is initially quite large in this case, up to 30% of the daily average production rate. By the fifth day, however, the models are in better agreement, and the mean rate of production is 16.3 ppbv d^{-1}, with an rms error of only about 2 ppbv d^{-1}, or 11%. To understand the Plume-X case, we have regrouped the 21 models into three subsets denoted A, B, and C. Again, the subsets were primarily defined with respect to similar relative abundances of O_3, HO_x, and NO_x. Three models did not obviously fall into any of the subsets and are denoted with an asterisk in Figure 8. The subsets in Figure 8 show a positive relation between concentrations of HO_x and the O_3 production rate; i.e., subset A shows highest values for O_3 and diurnally averaged HO_x (Figures 8a and 8c), while subset B shows the lowest values, and subset C results lie between. Additionally, there is an apparent negative relation between model to model differences in HO_x and NO_x and between differences in HO_x and the OH:HO_x ratio (subset A shows lowest values for NO_x and

Table 4. Diurnally Averaged HO_x Production Rates for Marine Case Subsets 2 and 3: Last Day of Integration

HO_x Production Pathway	Diurnal Mean Production of HO_x, molecules cm^{-3} s^{-1}	Root Mean Square Error, molecules cm^{-3} s^{-1}	Correlation (r) of Photolysis Rate to Diurnal HO_2 Mixing Ratio
$O_3 + h\nu \rightarrow O(^1D)$ $O(^1D) + H_2O \rightarrow 2OH$	5.9×10^5	$\pm 0.22 \times 10^5$	−0.11 (not significant)
$CH_2O + h\nu$ + fast steps $\rightarrow 2HO_2 + CO$	1.1×10^5	$\pm 0.30 \times 10^5$	+0.68 (significant to 99% confidence)
$H_2O_2 + h\nu \rightarrow 2OH + O_2$	3.0×10^5	$\pm 0.34 \times 10^5$	+0.54 (significant to 99% confidence)

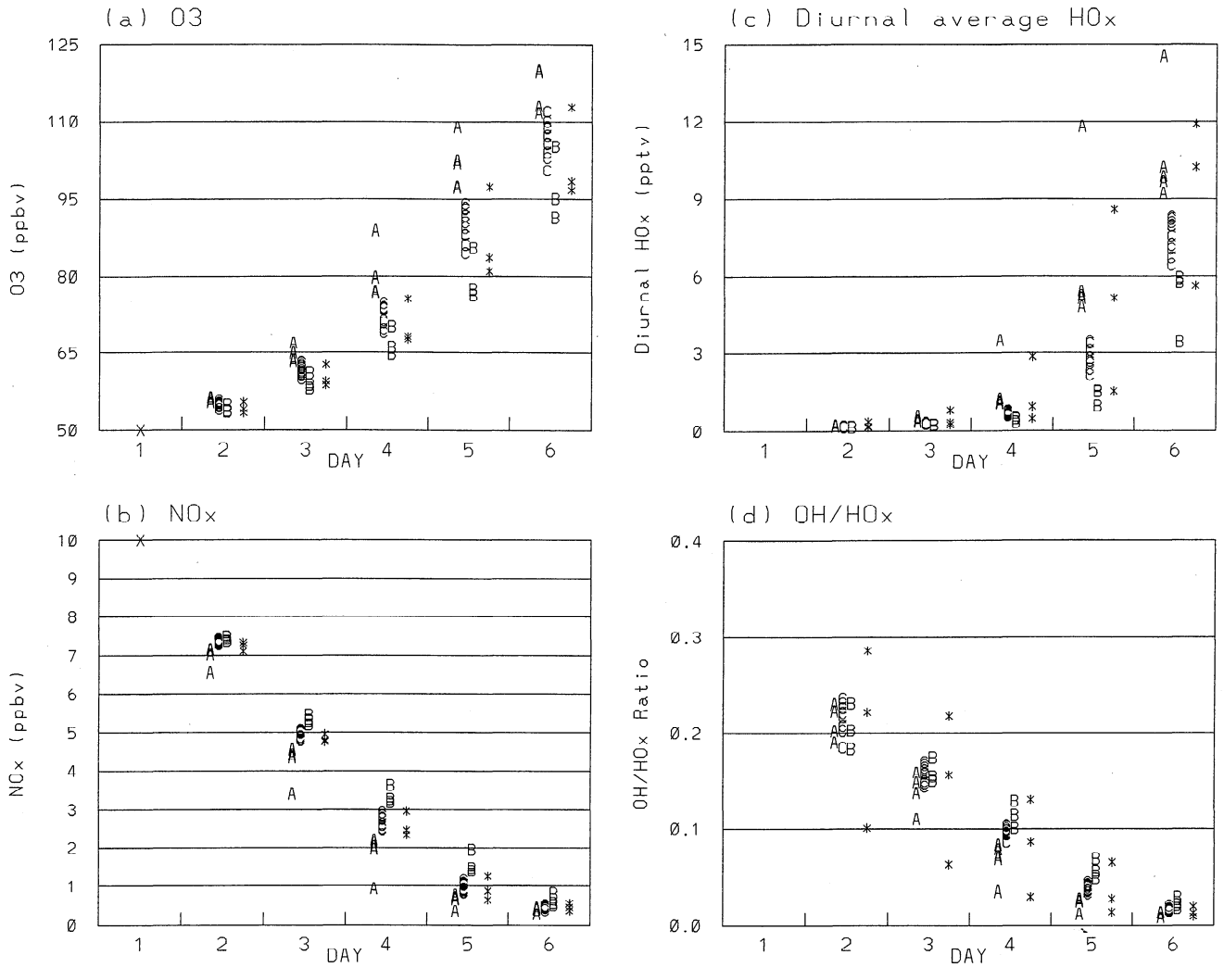

Figure 8. Individual model results for the Plume-X case. Each model is identified with a subset letter A, B, or C. Models that don't fit into any subset are shown with an asterisk. Noontime values for each day of the simulation (along the abscissa) are shown for (a) O_3 in ppbv and (b) NO_x in ppbv. Diurnally averaged values for the previous 24 hours are shown for (c) HO_x in pptv and (d) OH:HO_x ratio.

OH:HO_x, subset B shows the highest, and subset C lies between). These patterns of deviation are fully consistent with the general mean behavior of the NO_x and HO_x systems described above. This finding suggests that the factors that drive the model to model differences are related to the same parameterizations that control the mean photochemical behavior of HO_x in the high- and low-NO_x systems.

Figure 9 shows model calculated diurnal averages of photolysis rates for O_3, H_2O_2, and CH_2O at 4 km (the height of the Plume-X simulation). While there is no distinction between subsets for H_2O_2 and CH_2O photolysis (Figures 9b and 9c), there is a strong relation between the selected subsets and differences in the O_3 photolysis rates from the mean at this altitude. For instance, subset A, which shows highest values of HO_x, also clearly shows highest values for O_3 photolysis (Figure 9a). O_3 photolysis (followed by reaction of $O(^1D)$ with water vapor) accounts for about 80% of the HO_x source under these conditions and is expected to have a major impact on HO_x concentrations [see also *Thompson and Stewart*, 1991]. Table 5 lists the contribution to the total HO_x source from the photolysis of O_3, CH_2O, and H_2O_2. In this analysis the largest positive correlation between HO_2 and photolysis rates was calculated for O_3 photolysis. This calculation suggests that model to model differences in the HO_x sources that drive the differences in HO_x also subsequently have effects on the differences in NO_x and in the O_3 production rate for the Plume-X case.

4.3. Hydrocarbon Cases

There is no widely accepted standard for hydrocarbon oxidation schemes, as there is for inorganic chemistry and CO and CH_4 oxidation [*DeMore et al.*, 1992]. Most of the models here use NMHC oxidation schemes that are derived from one of three common sources, although many include model-specific modifications to these schemes: (1) the lumped molecule approach such as RADM-II [*Stockwell et al.*, 1990], (2) the lumped molecule with surrogate species approach [e.g., *Lurmann et al.*, 1986], and (3) the lumped structure approach

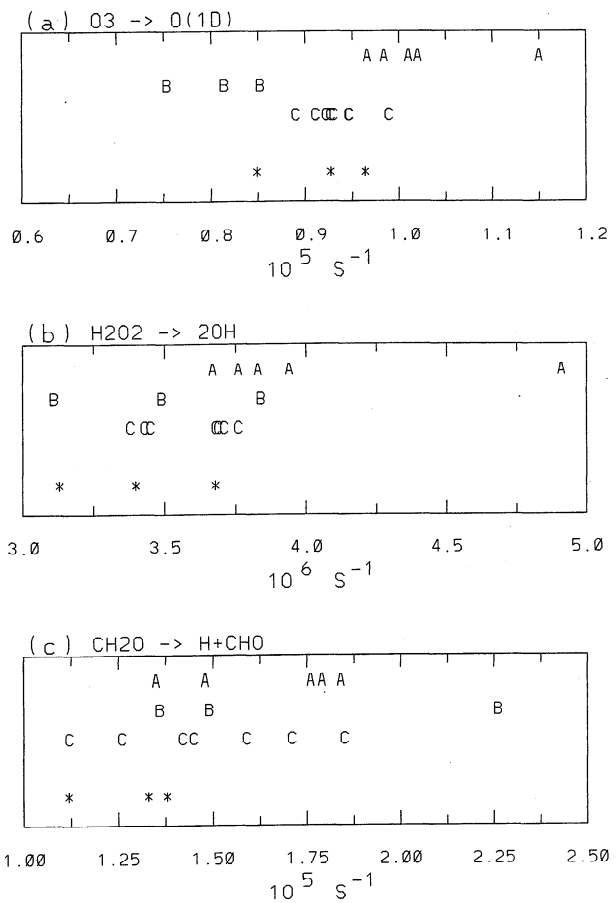

Figure 9. Diurnally averaged photolysis rates at 4 km. Rates are shown in inverse seconds for the diurnally averaged 4 km photolysis rate for (a) O_3 (to $O(^1D)$), (b) H_2O_2, and (c) CH_2O. Each model is identified with a subset number A, B, or C or with an asterisk, as in Figure 7.

such as Carbon-Bond IV [*Gery et al.*, 1989]. We find no obvious consistency of results as a function of these groups, however.

While the general trends of trace species are consistent within the group of 14 models that include results from the NMHC cases (e.g., large O_3 production at beginning of Plume-HC simulation, followed by a gradual decay), the scatter among the model results is quite large. Studies such as the one by *Hough* [1988] present a highly structured comparison of various mechanisms that focus on the specific hydrocarbon chemistry scheme used, removing as many other sources of variation as possible. As was discussed previously, such a comparison of photochemical oxidant mechanisms was not the intent of PhotoComp or in the scope of this report. Rather, we present the results for the Plume-HC and Land-Bio cases here (Figures 4 and 5) to illustrate the marked increased scatter of results produced by this group of models when NMHC chemistry is introduced.

The cases including hydrocarbons can be compared with the corresponding cases without NMHC chemistry, i.e., Land-Bio to the Land case and Plume-HC to the Plume-X case. In both instances the rms error for the predicted O_3 concentration on day 5 of the simulation is approximately doubled with the addition of NMHCs. The rms error for NO_x also increases dramatically, from 15% to nearly 40% in the Land/LandBio cases. The treatment of NMHC introduces a production of PAN and other nitrates into the system. Various treatments of these species are likely to contribute to the scatter of NO_x seen in Figures 4 and 5.

5. Summary

While PhotoComp was constructed with the specific goal to examine consistency among models for simple gas-phase photochemistry, the results reproduced some of the fundamental characteristics of tropospheric chemical processes previously described in the literature, such as the dependence of O_3 production on NO_x concentration and the nonlinear behavior of O_3 production efficiency per NO_x molecule as a function of NO_x concentration (e.g., 26 molecules of O_3 per additional molecule of NOx in the clean surface layer and 8–10 molecules of O_3 per molecule of NOx in the highly concentrated mid-troposphere plume).

Small but systematic differences were found between models in the simulation of the moist, lower tropospheric cases (e.g., Marine). These differences are important, because most of the global photochemical destruction of O_3 occurs in the remote lower troposphere under conditions similar to the Marine case. The 10% rms error for the net O_3 tendency in this case is primarily due to model to model differences in the rate of reaction of O_3 with HO_2. The differences in HO_2, in turn, can be traced to (1) inconsistent conversion rates for HO_2 to H_2O_2 due to some models leaving out the water vapor dependence for the self-reaction of HO_2 and (2) differences in the rates of

Table 5. Diurnally Averaged HO_x Production Rates for Plume-X Case; All Models: Last Day of Integration

HO_x Production Pathway	Diurnal Mean Production of HO_x, molecules cm^{-3} s^{-1}	Root Mean Square Error, molecules cm^{-3} s^{-1}	Correlation (r) of Photolysis Rate to Diurnal HO_2 Mixing Ratio
$O_3 + h\nu \rightarrow O(^1D)$ $O(^1D) + H_2O \rightarrow 2OH$	5.67×10^5	$\pm 0.90 \times 10^5$	+0.69 (significant to 99% confidence)
$CH_2O + h\nu$ + fast steps $\rightarrow 2HO_2 + CO$	0.84×10^5	$\pm 0.16 \times 10^5$	+ 0.13 (not significant)
$H_2O_2 + h\nu \rightarrow 2OH + O_2$	0.80×10^5	$\pm 0.37 \times 10^5$	+0.49 (significant to 99% confidence)

photodissociation reactions that are secondary sources of HO_x. While the choice of radiative transfer method had a significant impact on the rates of species that are photolytically destroyed in the longer wavelengths (NO_2 and CH_2O), this had little or no effect on the photolysis rates calculated for those species driven by the relatively shorter wavelengths (O_3 and H_2O_2).

In the middle tropospheric case (Plume-X) with high initial concentrations of NO_x a significant correlation was found between differences of HO_x from the mean and differences of the photolytic source term initiated by photolysis of O_3. These differences in turn affect the model-calculated decay of NO_x and the associated O_3 production rate, which had rms errors between 10% and 30%. Models predicted O_3 concentrations for the high-altitude Free case that were in closer agreement because of the slow chemistry under the prescribed conditions, but the rms error for O_3 tendency was about 20% of the decay rate. The introduction of hydrocarbons to the system further exacerbates the model to model differences, since NO_x then decays in less than a day to both HNO_3 and PAN, and the scatter between model results for both NO_x and O_3 increases. In both of the cases that consider hydrocarbons the rms error for O_3 concentration approximately doubled when NMHCs were included.

One of the most significant factors contributing to differences between these models is, not surprisingly, the radiative calculations for photolysis rates, which display typical rms errors of 5–15% of the mean. While it would be useful to pinpoint photodissociation rates in future intercomparisons such as this one in order to understand differences in chemistry, this error between models is still within the general range of accuracy for photokinetics data such as those of *DeMore et al.* [1992]. A useful next step might include a closer examination of model-generated diurnal cycles of photodissociation rates and a comparison of these with data.

The results from this intercomparison indicate that even for the simulation of extremely simple situations, there can be discrepancies in resulting constituent concentration and tendencies among model simulations that can be significant in some cases. Such model calculations are becoming increasingly important in assessments of future atmospheric composition and climate.

Acknowledgments. The authors wish to thank Keith E. Grant (LLNL), Douglas Kinnison (LLNL), Anne Gunn Kraabol (Norwegian Institute for Air Research), and Richard Stewart (NASA GSFC) for constructive comments and valuable technical and scientific assistance throughout the intercomparison.

References

DeMore, W. B., S. P. Sander, D. M. Golden, R. F. Hampson, M. J. Kurylo, C. J. Howard, A. R. Ravishankara, C. E. Kolb, and M. J. Molina, Chemical kinetics and photochemical data for use in stratospheric modeling: Evaluation number 10, *JPL Publ. 92-20*, 1992.

Dignon, J., and S. Hameed, Global estimates of nitrogen and sulfur oxides from 1860 to 1980, *J. Air Pollut. Control Assoc., 39*, 180–186, 1989.

Fehsenfeld, F., and S. Liu, Tropospheric ozone: Distribution and sources, in *Global Atmospheric Chemical Change*, edited by C. Hewitt and W. Sturges, pp. 169–231, Elsevier Sci., New York, 1993.

Fishman, J., J. M. Hoell Jr., R. D. Bendura, R. J. McNeal, and V. W. J. H. Kirchhoff, NASA GTE TRACE A Experiment (September-October, 1992): Overview, *J. Geophys. Res., 101*, 23,865–23,879, 1996.

Gery, M. W., G. Z. Whitten, J. P. Killus, and M. C. Dodge, A photochemical kinetics mechanism for urban and regional scale computer modeling, *J. Geophys. Res., 94*, 12,925–12,956, 1989.

Harris, N. R. P., et al.,: Ozone measurements, in *Scientific Assessment of Ozone Depletion: 1994*, chap. 1, *Rep. 37*, World Meteorol. Org. Global Ozone Res. and Monit. Proj., Geneva, Switzerland, 1995.

Harriss, R. C., et al., The Amazon Boundary Layer Experiment (ABLE 2A): Dry season 1985, *J. Geophys. Res., 93*, 1351–1360, 1988.

Hough, A. M., An intercomparison of mechanisms for the production of photochemical oxidants, *J. Geophys. Res., 93*, 3789–3812, 1988.

Isaksen, I. S. A., K. H. Midtbo, J. Sunde, and P. J. Crutzen, A simplified method to include molecular scattering and reflection in calculations of photon fluxes and photodissociation rates, *Geophys. Norv., 31*, 11–26, 1977.

Kahlil, M. A. K., and R. A. Rasmussen, Atmospheric methane: Trends over the last 10,000 years, *Atmos. Environ., 21*, 2445–2452, 1987.

Keeling, C. D., R. B. Bacastow, and T. P. Whorf, Measurements of the concentration of carbon dioxide at Mauna Loa Observatory, Hawaii, in *Carbon Dioxide Review 1982*, edited by W. C. Clarke, Oxford Univ. Press, New York, 1982.

Kircher, C. C., and S. P. Sander, Kinetics and mechanism of HO_2 and DO_2 disproportionations, *J. Phys. Chem., 88*, 2082–2091, 1984.

Kleinman, L. I., Seasonal dependence of boundary layer peroxide concentration: The low and high NO_x regimes, *J. Geophys. Res., 96*, 20,721–20,733, 1991.

Lelieveld, D., and P. J. Crutzen, Influences of cloud photochemical processes on tropospheric ozone, *Nature, 303*, 227–233, 1990.

Lin, X., M. Trainer, and S. C. Liu, On the nonlinearity of the tropospheric ozone production, *J. Geophys. Res., 93*, 15,879–15,888, 1988.

Liu, S. C., M. Trainer, F. C. Fehsenfeld, D. D. Parrish, E. J. Williams, D. W. Fahey, G. Hubler, and P. C. Murphy, Ozone production in the rural troposphere and the implications for regional and global ozone distributions, *J. Geophys. Res., 92*, 4191–4207, 1987.

Lurmann, F. W., A. C. Lloyd, and R. Atkinson, A chemical mechanism for use in long-range transport/acid deposition computer modeling, *J. Geophys. Res., 91*, 10,905–10,936, 1986.

Luther, F. M., Annual report of Lawrence Livermore National Laboratory to the FAA on the high altitude pollution program: 1980, *Rep. UCRL-50042-80*, Lawrence Livermore Natl. Lab., Livermore, Calif., 1980.

Madronich, S., Photodissociation in the atmosphere, 1, Actinic flux and the effects of ground reflections and clouds, *J. Geophys. Res., 92*, 9740–9752, 1987.

Meier, R. R., D. E. Anderson Jr., and M. Nicolet, Radiation field in the troposphere and stratosphere from 240-1000 nm, I, General analysis, *Planet. Space Sci., 30*, 923–933, 1982.

Möller, D., and G. Mauersberger, Cloud chemistry effects on tropospheric photooxidants in polluted atmosphere: Model results, *J. Atmos. Chem., 14*, 153–165, 1992.

Perner, D., U. Platt, M. Trainer, G. Huebler, and J. Drummond, Measurements of tropospheric OH concentrations: A comparison of field data with model predictions, *J. Atmos. Chem., 5*, 185–216, 1987.

Prather, M. J., R. Derwent, D. Ehhalt, P. Fraser, E. Sanheuza and X. Zhou, Other trace gases and atmospheric chemistry, in *Climate Change 1994*, edited by J. T. Houghton et al., Cambridge Univ. Press, New York, 1995.

Prinn, R., R. Weiss, B. Miller, J. Huang, F. Alyea, D. Cunnold, P. Fraser, D. Hartley, and P. Simmonds, Atmospheric trends and lifetime of trichloroethane and global average hydroxyl radical concentrations based on 1978–1994 ALE/GAGE measurements, *Science, 269*, 187–192, 1995.

Ridley, B. A., and E. Robinson, The Mauna Loa Observatory Experiment, *J. Geophys. Res., 97*, 10,285–10,290, 1992.

Salawitch, R. J., et al., The distribution of hydrogen, nitrogen, and chlorine radicals in the lower stratosphere: Implications for changes in O_3 due to emission of NO_y from supersonic aircraft, *Geophys. Res. Lett., 21*, 2547–2550, 1994.

Sillman, S., J. A. Logan, and S. C. Wofsy, The sensitivity of ozone to nitrogen oxides and hydrocarbons in regional ozone episodes, *J. Geophys. Res., 95*, 1837–1851, 1990.

Stockwell, W. R., On the HO_2+HO_2 reaction: Its misapplication in atmospheric chemistry models, *J. Geophys. Res., 100*, 11,695–11,698, 1995.

Stockwell, W. R., P. Middleton, J. S. Chang, and X. Tang, The second-generation Regional Acid Deposition Model chemical mechanism for

regional air quality modeling, *J. Geophys. Res., 95*, 16,343–16,367, 1990.

Stolarski, R. S., et al., 1995 scientific assessment of the atmospheric effects of stratospheric aircraft, *NASA Ref. Publ. 1381*, 1995.

Stordal, F., R. G. Derwent, I. S. A. Isaksen, D. Jacob, M. Kanakidou, J. A. Logan, and M. J. Prather, Model simulations of global tropospheric ozone, in *Scientific Assessment of Ozone Depletion: 1994*, chap. 7, *Rep. No. 37*, World Meteorol. Org. Global Ozone Res. and Monit. Proj., Geneva, Switzerland, 1995.

Thompson, A. M., The oxidizing capacity of the Earth's atmosphere: Probable past and future changes, *Science, 256*, 1157–1165, 1992.

Thompson, A. M., and R. W. Stewart, Effect of chemical kinetics uncertainties on calculated constituents in a tropospheric photochemical model, *J. Geophys. Res., 96*, 13,089–13,108, 1991.

Volz, A., and D. Kley, Evaluation of the Montsouris series of ozone measurements made in the nineteenth century, *Nature, 332*, 240–242, 1988.

T. Berntsen, University of Oslo, Oslo, Norway N-1305.

G. Carmichael, Univeristy of Iowa, Iowa City, IA 52240.

R. Chatfield, NASA Ames Research Center, Moffett Field, CA 94035.

P. Connell, Lawrence Livermore National Laboratory, Livermore, CA 94550.

R. Derwent, Meteorological Office, Bracknell, Berkshire, RG12 2SZ England.

L. Horowitz, Harvard University, Cambridge, MA 02138.

S. Jin, New York State Department of Transportation, New York, NY 12232.

M. Kanakidou, Centre des Faibles Radioactivites, Gif-sur-Yvette Cedex, France.

P. Kasibhatla, MCNC/Environmental Programs, Research Triangle Park, NC 27709.

R. Kotomarthi, AER, Inc., Cambridge, MA 02139.

M. Kuhn, Fraunhofer Institut fuer Atmosphaerische Umweltforschung, Garmisch-Partenkirchen, Germany D-82467.

K. Law, Cambridge University, Cambridge, CB2 1EW England.

J. Olson, NASA Langley Research Center, Hampton, VA 23681. (e-mail: j.r.olson@larc.nasa.gov)

L. Perliski, Geophysical Fluid Dynamics Laboratory, Princeton, NJ 08542.

M. Prather, University of California Irvine, Irvine, CA 92717.

S. Sillman and J. Penner, University of Michigan, Ann Arbor, MI 48109.

F. Stordal, Norwegian Institute for Air Research, Kjeller, Norway N-2007.

O. Wild, NASA Goddard Space Flight Center, Greenbelt, MD 20771.

(Received March 27, 1996; revised October 11, 1996;
accepted October 28, 1996).